

# COMMISSIONING BEAM-LOSS MONITORS FOR THE SUPERCONDUCTING UPGRADE TO LCLS\*

Alan S. Fisher<sup>†</sup>, G. W. Brown, E. P. Chin, C. I. Clarke, W. G. Cobau, T. Frosio, B. T. Jacobson, R. Kadyrov<sup>\*\*</sup>, J. A. Mock, Jino Park, E. Rodriguez, P. K. Roy, M. Santana Leitner, J. J. Welch  
SLAC National Accelerator Laboratory, Menlo Park, CA, USA

## Abstract

Commissioning of the 4-GeV, 120-kW superconducting linac, an upgrade to the LCLS x-ray FEL at SLAC, began in summer 2022, by accelerating a beam through the first cryomodule to 100 MeV. This autumn the beam will accelerate along the full linac, pass through the bypass transport line above the copper linac, and end at a new high-power tune-up dump at the muon shield wall. The first beam through the undulators is expected by early 2023, at a rate well below the full 1 MHz. A new system of beam-loss detectors will provide radiation protection, machine protection, and diagnostics. Radiation-hard optical fibres span the full 4 km from the electron gun to the undulators and their beam dumps. Diamond detectors cover anticipated loss points. These replace ionization chambers previously used with the copper linac, due to concern about ion pile-up at high loss rates. Signals from the new detectors are integrated with a 500-ms time constant and compared to the allowed threshold. If this level is crossed, the beam stops within 0.2 ms. We report on the initial commissioning of this system and on the detection of losses of both photocurrent and of dark current from the gun and cryomodules.

## INTRODUCTION

SLAC removed the first km of its 3-km copper electron linac, completely emptying this part of the tunnel and the Klystron Gallery above it for the first time since construction in the 1960s. The LCLS-II Project replaced this with a new superconducting (SC) linac with 35 12-m-long cryomodules operating at  $f_{RF} = 1.3$  GHz and two third-harmonic cryomodules. All have been installed in the first 700 m of this 1-km section of the tunnel (Fig. 1 of [1]).

In addition, two variable-gap undulators, for hard and soft x-rays, replaced the fixed-gap LCLS undulator. Both are in use with beam from the LCLS normal-conducting (NC) copper linac, in the third km. With a complex arrangement of bend magnets and kickers, one linac can share its rate between the two undulators, or the SC beam can go to one undulator and the NC beam to the other.

The SC linac, driven with continuous-wave (CW) RF power, will produce 4-GeV bunches with variable spacing at 1 MHz ( $f_{RF}/1400$ ). The risk of damaging beam loss grows as the maximum operational beam power jumps from 500 W for the NC linac to 120 kW. A planned energy upgrade (LCLS-II-HE) will install more cryomodules with higher gradients, doubling the beam energy to 8 GeV and so doubling the beam power and the potential for damage.

\* SLAC is supported by the U.S. Department of Energy, Office of Science, under contract DE-AC02-76SF00515.

<sup>†</sup> afisher@slac.stanford.edu

<sup>\*\*</sup> Present address: Apple Inc., Cupertino, California

The SC photoinjector is driven by CW RF at 186 MHz ( $f_{RF}/7$ ) with a 1.3-GHz buncher. This source generates 750-keV electron bunches, which enter the first cryomodule (CM01) after 3 m. Each cryomodule has 8 RF cavities and operates at a temperature of 2 K.

At this time (early September 2022), photocurrent at 10 Hz passed through CM01 and reached energies from 80 to 100 MeV. The commissioning path then terminated the beam at collimator CYC01 (56 m from the cathode, Fig. 1), which was locked with its jaws closed. Alternatively, bunches have been kicked into the DIAG0 diagnostic line that can sample the full-rate beam at up to 120 Hz.

In October 2022, we plan to commission the 3.2 km path from the gun to the tune-up dump in the beam switchyard (BSY). Beam may travel through the undulators to their beam dumps for the first time by the start of 2023.

## LONG BEAM-LOSS MONITORS

SLAC has depended on ion chambers [1] for loss measurements, to cover extended regions and points of known loss, such as beam stoppers or collimators. Simulations [1] have demonstrated that at high loss rates ions piling up in these devices may blind them to further losses. This consideration and others led to the adoption of new designs using Cherenkov emission in quartz optical fibres as Long Beam-Loss Monitors (LBLMs), and electron-hole pairs in diamond chips as Point Beam-Loss Monitors (PBLMs) [1]. This paper reports only on the LBLM performance during early commissioning through CM01, since most PBLMs are in the high-energy region that has not yet seen beam.

## LBLM Design

As an electromagnetic shower from beam loss passes through the radiation-hard quartz optical fibre, it emits Cherenkov light traveling both upstream and downstream. A photomultiplier tube (PMT) is placed at the fibre's downstream end to detect this light, since our tests found 4 times more signal in this direction [1]. The PMT is in a rack-mounted chassis outside the tunnel, to be accessible and near the signal-processing electronics (Fig. 7 of [1]). At the fibre's upstream end, an LED emits weak light modulated at 0.8 Hz. A digital signal processor (DSP) detects this "self-check" or "heartbeat" using a sensitive filter based on a digital lock-in amplifier. This frequency is below any beam rate and is shared through the power line ( $(60 \text{ Hz})/75 = 0.8 \text{ Hz}$ ) by the LED and DSP. The red-sensitive PMT (Hamamatsu H7422P-40) is housed in a Peltier-cooled module operating at 0°C to limit dark current [1].

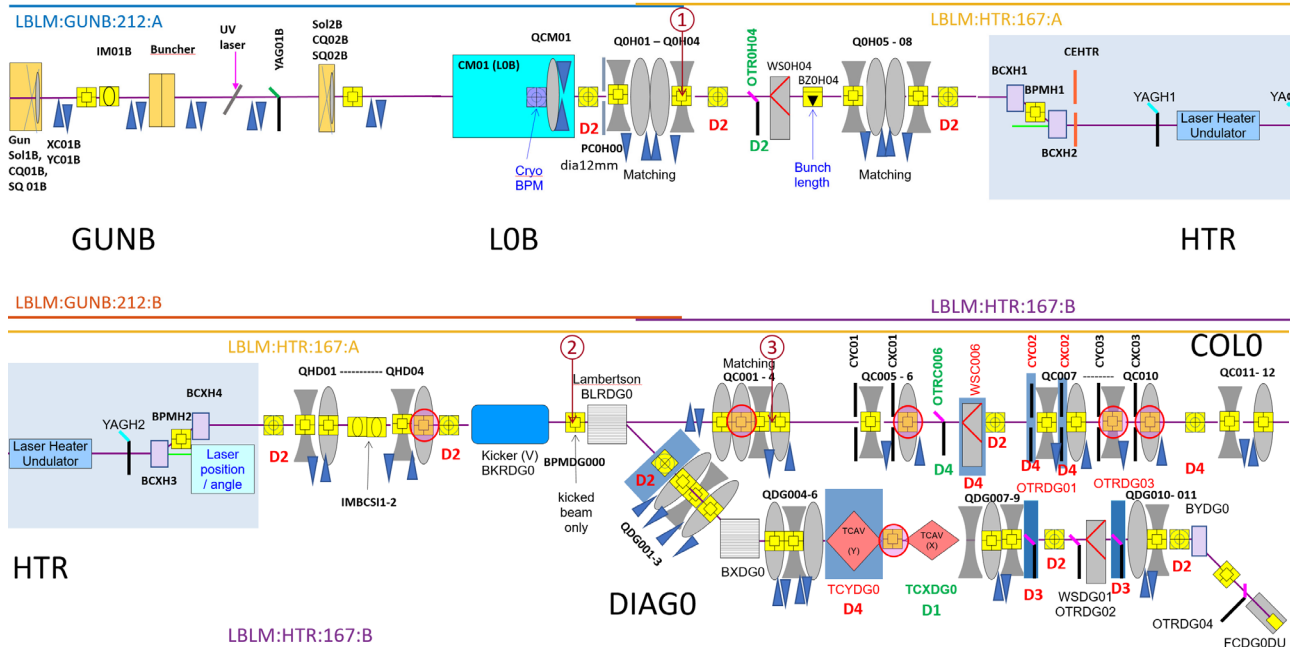


Figure 1: During the initial commissioning period, L0B (CM01, the first cryomodule) accelerated electrons from the 750 keV gun to a maximum of 100 MeV. The beam passed through the laser-heater chicane (without undulator or laser) and entered the first collimation region COL0. Collimator CYC01 was locked closed to stop the beam. Bunches could also be kicked into diagnostic beamline DIAG0, designed to sample a high-rate beam at up to 120 Hz. The three circled numbers show locations where bunch bursts were steered into the beampipe to test the LBLMs. The coverage of the four fibres in this region is shown. The HTR fibres end further downstream.

### LBLM Locations

LBLMs cover the full 4-km path from the gun (GUNB) to the undulator beam dumps. The fibre length is typically 200 m, but lengths are adjusted to span a functional zones such as linac L2B (cryomodules between the first and second bunch compressors BC1B and BC2B, where the “B”

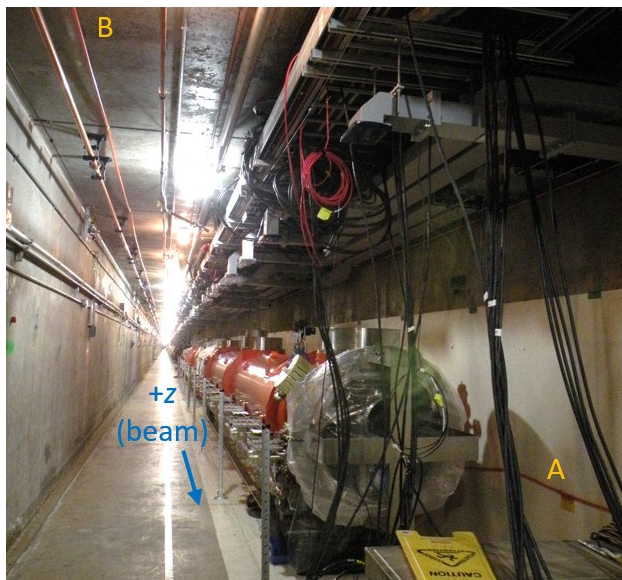


Figure 2: Photo during installation showing the A fibre on the right (north) wall and the B fibre on the ceiling at left. Both are in 6-mm orange “fibre ducts” that allow fibre replacement in a few minutes, without entering the tunnel.

suffix distinguishes the SC machine from similar sections of the NC machine). To provide redundancy and different viewing angles, all SC linac regions have two fibres on separate shut-off chains. This linac, which runs from west to east, has A-Chain fibres on the north wall at beam height and 90 cm (transversely) from the beam, and B-Chain fibres on the tunnel ceiling toward the south wall, 3 m from the beam (Fig. 2). To compensate for the greater distance, PMTs for B-Chain fibres operate at a higher voltage.

Two fibre pairs span the region just commissioned (Fig. 1). The GUNB pair starts upstream of the gun and continues 8 m past linac L0B (CM01). The HTR fibres cover the laser-heater region. They overlap the GUNB fibres by 4 m and continue for 68 m, past collimator CYC01 that ended the beam path for 100-MeV commissioning.

### Dark Current from the Gun

The gun energy, 750 keV, is near the 200-keV Cherenkov threshold in the quartz fibres and is too low to create radiation showers. Consequently, no LBLM signal has been seen from the gun and buncher alone. After acceleration in L0B, beam losses produce strong signals.

Dark current - with the gun, buncher, and L0B all on, but without photocathode laser pulses - can be seen on both the GUNB and HTR fibres, but especially on the HTR pair due to their much longer path after L0B. Adjustments upstream of CM01 have a strong effect. In Fig. 3, a motor moves a “ladder” of collimating apertures upstream of L0B. A Ce:YAG screen on the ladder shows “hot spots” of dark current from the cathode rim imaging to a radius between 10 and 12 mm. A 24-mm aperture passes this dark current

Content from this work may be used under the terms of the CC BY 4.0 licence (© 2022). Any distribution of this work must maintain attribution to the author(s), title of the work, publisher, and DOI

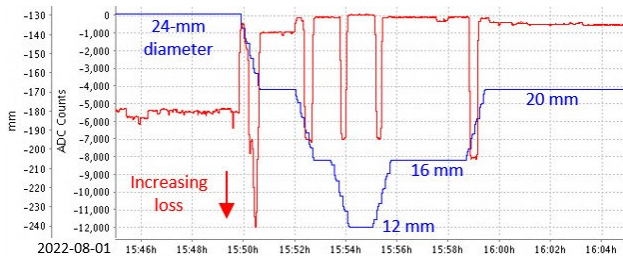


Figure 3: Gun dark current (red) seen by the HTR B fibre as a motor (blue) changes collimating apertures, 1 m before CM01. Loss signals are negative and go downward. Strong loss also appears when the motor is between apertures.

into L0B, creating a strong loss signal. The 20-mm aperture cuts dark current significantly. The 16-mm and 12-mm apertures limit it even more but require tighter focusing of the photocurrent. A small reduction in the field of the focusing solenoid at the gun also raises dark-current losses.

### Burst of Photocurrent Bunches

Single bursts of 500 bunches of photocurrent were produced with 2- $\mu$ s bunch spacing (1 ms burst length), each with 220 pC at 80 MeV (18 mJ each, 8. J total). Corrector magnets directed this beam at grazing incidence onto the beampipe at three locations (Fig. 1) in the 38 m between protection collimator PC0H00 and halo collimator CYC01.

Figure 4 shows the LBLM responses at Location 1. Charge from each bunch accumulates on the integration capacitor and decays with a 500-ms RC time constant. The correctors here could make a loss only in the +x (north) direction. The forward angle of the loss shower brings it to the ceiling past the end of the B fibre of the GUNB pair, giving this fibre a weak signal. All show a pedestal consisting of an ADC offset for each channel, soon to be measured and subtracted; dark current, which was kept low in this test by using the 20-mm aperture and a sufficiently high solenoid field; and the small 0.8-Hz modulation of the self-check LED.

Figure 5 summarises all locations and loss directions. Locations 2 and 3 are too far downstream for the GUNB fibres to detect their losses. Shielding by local structures is evident in the weaker response at Location 2, especially for the HTR A fibre. Here the loss was on the -x (south) side, away from the wall, suggesting a directional effect. At Location 3, the correctors allowed losses in three directions, -x and +y (up), and -y. The response of the ceiling fibre was greater for downward, not upward, loss, which may indicate that the direction of the loss is less important than details of local showering and shielding. The -x losses at Locations 2 and 3 show that one fibre in a pair can compensate for a weak signal from the other, demonstrating the value of redundancy with two viewing angles.

A beampipe hit at grazing incidence can present a “thin” target: the resulting electromagnetic shower mostly escapes. We will next test thick targets, such as collimators. In FLUKA simulations, these signals could be as much as 50 times weaker, depending on target shape, but a preliminary look at loss from scraping on PC0H00 showed only a factor of 3. Because this collimator has a central aperture

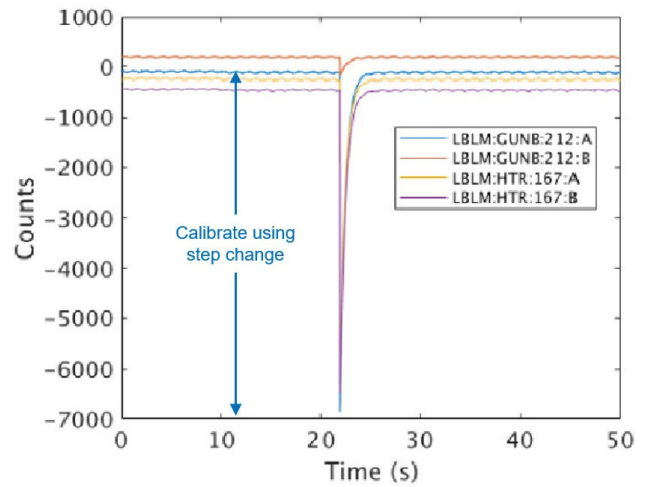


Figure 4: Loss of a 500-pulse burst (8.8 J) at grazing incidence on the beampipe at Location 1. A signal of 1 mV at the digitiser input corresponds to 25.2 ADC counts.

to pass photocurrent, some of the loss seen may have been caused by scraping on the beampipe rather than a pure thick-target loss.

BCS were tested at Location 1 with the three fibres that gave strong responses (Fig. 4). Bursts of 500 bunches were fired as the trip level was moved between 90 and 500 mV. Whenever the signal exceeded the trip threshold, trip requests went through the logic to the shut-off control.

### Initial Calibration

These measurements provide a preliminary calibration relating the lost beam energy to the loss signal. Figure 5 shows a typical signal level of 75 mV for the loss of 8.8 J in the 1-ms burst. However, if the bunches making this loss arrive uniformly in time, at a steady 17.6 W, then the capacitor charge from earlier bunches will decay with the 500-ms time constant, lowering the peak after 500 ms by the factor  $(1 - e^{-1})$ . The typical signal should be reduced to 47.4 mV, or 2.7 mV/W.

Compare this level to the safety thresholds specified by the Radiation Physics group. In the linac, the Beam Containment System (BCS, which protects both personnel outside the tunnel and radiation-safety components inside)

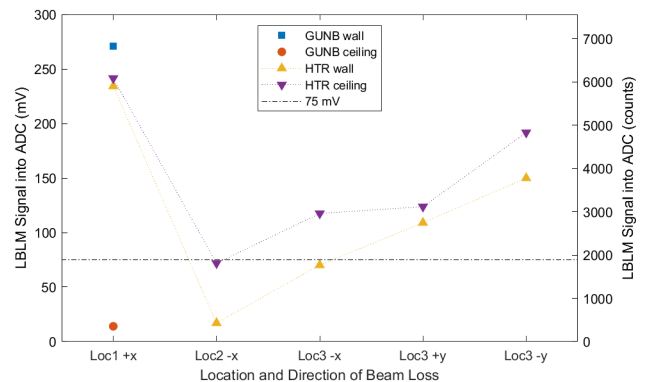


Figure 5: LBLM signals from grazing-incidence beam loss at 3 locations, in the directions indicated. Correctors could make a loss in more than one direction at Location 3 only.

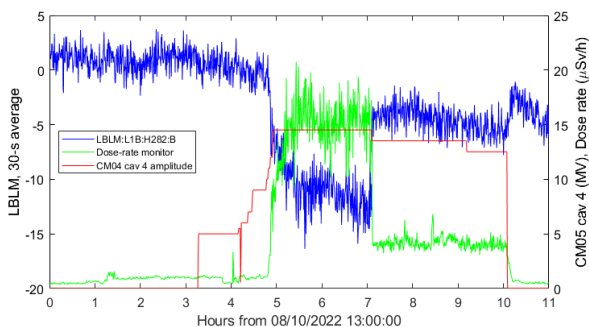


Figure 6: Comparing an LBLM (30-s average) to the RF in cavity 4 of CM05 and to a radiation dose-rate monitor.

must trip (shut off) the beam for losses above 1 kW. A BCS trip shuts the laser but also shuts off RF to L0B, which makes recovery slow. The Machine Protection System (MPS, which protects accelerator hardware) recovers quickly and is intended to trip first, with a threshold that is usually 10 times lower - 100 W in the linac.

The measured signals are strong at levels well below these thresholds. In fact, scaling to the BCS level of 1 kW gives 2.7 V, exceeding the maximum of 2 V in the BCS hardware. However, thick targets will lower this calibration. Ultimately trip levels will be reconsidered with data from tests in which losses are made at frequent intervals throughout the beam path.

### Field Emission from Cryomodules

The cryomodule for CM01 was selected for low field emission, since electrons emitted there can closely match the photocurrent in energy and pass through the full linac, leading to damage at high energy. We have not seen field emission from CM01, but it has not been on without gun RF too, and the gun's dark current dominates the signal.

A more revealing test of the sensitivity of the LBLMs to field emission came when all cryomodules (except the harmonic modules) were turned on for several hours and their gradients gradually raised. RF experts noted that cavity 4 of CM05 began emitting above 12 MV (Fig. 6). A radiation monitor measured a dose rate of 20  $\mu\text{Sv/h}$ . This small emission was also observed by LBLM:L1B:H282:B, but at a level of 12 counts rather than the thousands from burst losses. Consequently, the signal was averaged in 30-s bins (24 periods of 0.8 Hz) to filter the self-check modulation.

This B fibre is on the ceiling and ends 13.6 m upstream of the cavity. The A fibre of the pair did not see the signal, nor did the next fibre pair, which runs along this cavity. Note that the phases of the cavities were not adjusted for acceleration but were random. This phasing may have promoted backward acceleration toward the end of fibre H282:B. Alternatively, another cavity may also have been emitting during this interval, since many gradients were changed at nearly the same time. A dedicated study of field emission is needed in which the amplitude of a suspect cavity is raised and lowered independently.

### Fast Waveform for Diagnostics

In addition to beam containment and machine protection, the LBLMs were designed for a third application. The

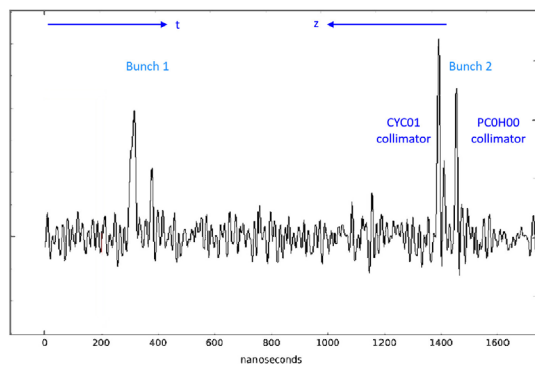


Figure 7: Fast waveform digitizer, showing two bunches 1  $\mu\text{s}$  apart. Each scrapes upstream collimator PCOH00 and ends at collimator CYC01, 38 m downstream. Bunch 2 arrives after bunch 1, but for each the downstream loss reaches the PMT first.

passive filter/splitter that provides  $RC$  integration of the low frequencies in the signal also sends frequencies above 1 MHz to a fast waveform digitizer. The arrival time of the signal at the PMT then indicates the loss location (Fig. 7).

Electrons travel at speed  $c$  along the beamline to the loss point, but the Cherenkov light travels in the fibre at  $c/n$ , where  $n$ , the refractive index, is 1.45. With the PMT at the downstream end of the fibre, signals from two loss points separated by a distance  $L$  arrive separated in time by  $\Delta t_d = -(n-1)L/c$ . The sign indicates that the upstream loss arrives before the downstream, so that the signs of their linac coordinate  $z$  and of arrival time  $t$  are opposite. With the PMT at the upstream end, the arrival-time difference,  $\Delta t_u = +(n+1)L/c$ , is approximately 5 times greater.

Despite lower  $z$  resolution, we chose the downstream position to gain the factor of 4 in signal strength noted earlier. Since the PMT itself is fast, with a 1-ns rise time, fast electronics could provide finer resolution, but the digitiser's 350-MSamp/s rate and 80-MHz anti-aliasing filter slow its response. Overshoot is also visible in Fig. 7. Two improvements are under consideration: the sample rate can be raised to 380 MHz (although the anti-aliasing filter may limit the benefit), and we have begun testing a deconvolution of the overshoot. Nevertheless, the figure shows a clear separation of two peaks from collimators 38 m apart.

## CONCLUSIONS

The LBLMs have demonstrated a strong and robust response to losses of both photocurrent and gun dark current at 80 MeV. They provide good coverage but with variations from local shielding. The onset of field emission from cryomodules has been observed. Waveforms for beam-loss localization have been seen. Testing will resume with thick targets before continuing through the full linac to 4 GeV.

## REFERENCES

- [1] A. S. Fisher *et al.*, "Beam-loss detection for the high-rate superconducting upgrade to the SLAC Linac Coherent Light Source", *Phys. Rev. Accel. Beams*, vol. 23, p 082802, 2020. doi: 10.1103/PhysRevAccelBeams.23.082802